Optics Letters

Thermally tunable ultracompact Fano resonator on a silicon photonic chip

Weifeng Zhang and Jianping Yao*

Microwave Photonic Research Laboratory, School of Electrical Engineering and Computer Science, University of Ottawa, 800 King Edward Avenue, Ottawa, Ontario K1N 6N5, Canada
**Corresponding author: jpyao@eecs.uottawa.ca*

Received 28 August 2018; revised 7 October 2018; accepted 7 October 2018; posted 10 October 2018 (Doc. ID 344267); published 29 October 2018

A thermally tunable ultracompact Fano resonator on a silicon photonic chip is reported. The Fano resonator is implemented by using an add–drop microdisk resonator (MDR) with the through and drop ports connected by two waveguides and combined via an adiabatic 2 × 2, 3 dB coupler to form a Mach–Zehnder interferometer (MZI). Due to the resonant mode interference between the MDR and the MZI, a Fano resonance with an asymmetric line shape resulted. A *p*-type-doped microheater is incorporated in the MDR to achieve thermal tunability. By tuning the direct current (DC) voltage applied to the microheater, the Fano resonance is tuned. The proposed Fano resonator is designed, fabricated, and characterized. Measurement results show that a Fano resonance with an extinction ratio of 30.2 dB and a slope rate of 41 dB/nm is achieved. When the microheater is tuned by tuning the DC voltage with a power from 0 to 22.9 mW, the Fano line shape is largely tuned with the Fano parameter *q* tuned from negative to positive and a maximum wavelength shifting as large as 15.97 nm. Thanks to its ultracompact configuration, and strong and fast tunability with low power consumption, the integrated Fano resonator holds a high potential for applications such as on-chip optical switching and sensing.

https://doi.org/10.1364/OL.43.005415

Fano resonance occurs when a discrete quantum state interferes with a continuum band of states [1]. Because of its sharp asymmetric line shape, Fano resonance has received considerable attention [2] and has been employed for applications such as high-sensitivity sensing [3], low-power optical switching, and high-efficiency optical modulation [4,5]. Fano resonators can be implemented based on different material systems [6,7]. Thanks to its compatibility with the current CMOS fabrication technique, silicon photonics is becoming one of the most promising photonic integrated platforms for low-cost, high-volume, and reliable manufacturing and for significant potential integrating with electronics [8]. Numerous silicon-based solutions have been proposed to implement Fano resonators [9–13]. These solutions are based on slot waveguides [9], Bragg waveguide gratings [10,11], microring resonators (MRRs) [12], and photonic crystal cavities [13]. However, the main problem associated with these solutions is that the Fano resonance cannot be tuned after the device is fabricated, which imposes a rigid limitation on its applications.

To overcome this problem, different tuning mechanisms have been proposed to realize a Fano resonator with tunable resonance [14–19]. Recently, we have proposed and demonstrated an optically tunable Fano resonator based on a grating-based Fabry–Perot cavity-coupled MRR [14]. With the use of two-photon absorption in silicon, the Fano resonance could be optically tuned. The tuning speed is fast, in the order of milliseconds, but the tuning range is limited. In addition, the optical performance is degraded due to the increase in free-carrier optical absorption loss resulted from two-photon absorption. In Refs. [15,16], a nanoelectromechanical system (NEMS) was used to tune the Fano resonance in a photonic crystal cavity. The main limitation is again the small tuning range. Thanks to the high thermo-optic coefficient in silicon, thermal tuning of the Fano resonance with a large tunable range is possible. In Refs. [17,18], a metallic microheater was placed on top of a Fano resonance device for thermal tuning. In Ref. [17], based on the interference of two resonant beams in an MRR, a Fano resonance was demonstrated experimentally, and its line shape was tuned by controlling the phase difference between the two beams with the use of a microheater. However, the device has a multimode interferometer (MMI) and a waveguide crossing, which makes the device complicated. In addition, the MRR has a larger radius with higher power consumption as compared with a microdisk resonator (MDR). For future high-density and large-scale photonic-integrated circuits (PICs), an individual device with a small footprint and a low power-consumption is highly needed, since it would elevate the integration density and power efficiency of an entire chip.

In this Letter, we propose and demonstrate a thermally tunable ultracompact Fano resonator on a silicon photonic chip. In the chip, an add–drop MDR is employed, in which the through and drop port waveguides are connected via two waveguides and combined via an adiabatic 2 × 2, 3 dB coupler to form a Mach–Zehnder interferometer (MZI). Due to the

interference between the resonant modes from the MDR and the MZI, a Fano resonance with an asymmetric line shape is produced. To achieve thermal tuning, a *p*-type-doped microheater is incorporated in the MDR. By applying a tunable direct current (DC) voltage, the Fano resonance is tuned. Measurement results show that a Fano resonator with a resonance having an extinction ratio of 30.2 dB and a slope rate of 41 dB/nm is achieved. When the microheater is tuned with a power from 0 to 22.9 mW, the Fano line shape is largely tuned with the Fano parameter q tuned from negative (−0.98) to positive (0.95), and with a maximum resonance wavelength tuning range of 15.97 nm. The key advantage of the proposed device is its ultracompact configuration and strong and fast tunability with low power consumption, which makes this integrated Fano device hold a high potential for applications in on-chip optical switching and sensing.

Figure 1(a) illustrates the perspective view of the proposed integrated Fano resonator on a silicon photonic chip. A lightwave signal is launched into the chip via an input grating coupler and sent to the add–drop MDR. Within the MDR, the input lightwave signal is split and directed to the through and drop ports. The two lightwave signals then pass through two waveguides and combine at an adiabatic 2 × 2, 3 dB coupler, which forms an MZI. At the output of the coupler, one part of the combined lightwave signal is sent to an output grating coupler for real-time optical monitoring, and the other part of the combined lightwave signal is sent to a Germanium-doped PIN photodetector. At the add port of the MDR, to avoid unwanted optical reflection, a waveguide terminator is employed. The length difference between the through and drop paths is designed to be 38.4 μm, and thus the MZI has a free spectral range (FSR) of 7.1 nm. To achieve Fano resonance tuning, a *p*-type-doped microheater is incorporated in the disk.

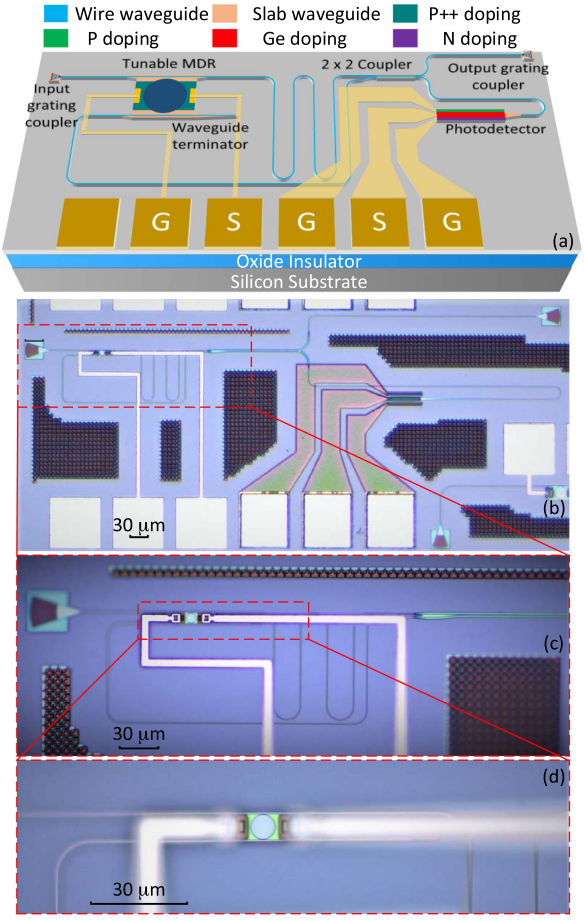

Fig. 1. (a) Perspective view of the proposed Fano resonator on a silicon photonic chip. (b) Image of the device. (c) Zoom-in view of the MDR, the two waveguides, and the 2 × 2 coupler. (d) Zoom-in view of the add–drop MDR with a doped microheater.

The device is fabricated using a CMOS-compatible technology with 193-nm-deep ultraviolet lithography. The wire waveguide with a width of 500 nm is employed as the fundamental waveguide structure. Figure 1(b) shows the microscope image of the fabricated Fano device. As can be seen, the through path is designed to have a longer waveguide transmission length. This is because the lightwave signal at the drop port would suffer from a larger optical insertion loss. A longer waveguide length at the through port is used to balance the optical loss difference between the through and drop paths. The entire device has a length of 850 μm and a width of 390 μm, a total area of 0.33 mm^2, as shown in Fig. 1(b). Figure 1(c) gives a zoom-in view of the MDR, the two waveguides, and the 2 × 2 coupler. The MDR has a radius of 3.7 μm with an identical coupling gap of 200 nm between the disk and two bus waveguides. Figure 1(d) shows a zoom-in view of the MDR. A *p*-type doped microheater is incorporated in the disk for thermal tuning. Compared with the top-placed metallic microheater, the doped microheater has a higher power efficiency.

We first study the operation of the device based on simulations. The transfer matrix method is used to simulate the transmission spectral response of the proposed Fano device, and a typical simulation result is shown in Fig. 2(a). Thanks to the resonant mode interference between the MDR and the MZI, a Fano resonance with an asymmetric line shape is produced, of which the Fano parameter q is negative. When the radius of the MDR is increased, its resonance wavelength is redshifted. Since the resonance of the MZI is maintained unchanged, the optical interference between the mode of the MDR and the MZI is tuned, and thus the Fano resonance is also tuned. As can be seen in Fig. 2(b), with the increasing in

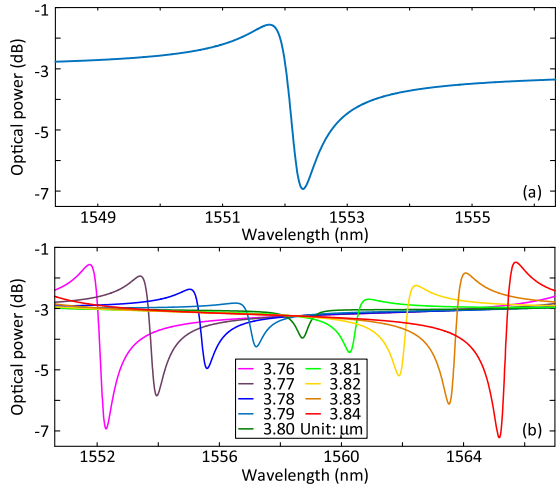

Fig. 2. (a) Simulated Fano resonance of the proposed device. (b) Fano resonance tuning with the radius of the MDR increasing.

the radius of the MDR, the Fano resonance is redshifted, and its Fano parameter q is tuned from negative to positive. When the Fano parameter q is equal to zero, which indicates that there is no optical interference between the resonant modes of the MDR and the MZI, a resonant notch of the MDR is presented. The optical interference between the resonant modes of the MDR and the MZI results in a Fano resonance, and this optical interference determines the line shape of the Fano resonance or the Fano parameter q [2], which could be adjusted by changing the radius of the MDR or the length difference between the two arms of the MZI.

The MDR in the device plays a critical role in achieving the Fano resonance. To evaluate the optical performance of the entire Fano device, the performance of the add–drop MDR is first evaluated. To do so, we fabricate a stand-alone add–drop MDR with identical parameters as the one in the Fano device. Figure 3(a) shows the perspective view of the add–drop MDR. A symmetric configuration is used, to make the coupling gaps between the disk and two bus waveguides identical. To increase the wavelength selectivity, the MDR is specifically designed to incorporate an additional slab waveguide to wrap the disk and the lateral sides of the bus waveguides, which is of help in decreasing the scattering loss of the confined optical field due to the disk sidewall roughness and in enhancing the optical coupling between the disk and the bus waveguides [20]. Figure 3(b) shows the cross-sectional view of the MDR along the white dashed line AA′ in Fig. 3(a). The MDR has a radius of 3.7 μm, which is much smaller than the minimum radius of an MRR ever reported, and the coupling gap is designed to be 200 nm. To meet the phase-matching condition, the width of the bus waveguide is 470 nm to effectively excite the first-order whispering gallery mode (WGM). To achieve thermal tuning, a p-type-doped microheater is incorporated in the MDR. To avoid the thermal impact on the optical coupling between the disk and the bus waveguides, the width of the incorporated microheater is designed to be 3.45 μm, smaller than the disk radius. Figure 3(c) shows the fabricated add–drop MDR. Four integrated waveguide-to-fiber grating couplers placed uniformly on the chip with an identical spacing of 127 μm are used to couple light into or out of the chip through a fiber array. Figure 3(d) shows the zoom-in view of the MDR.

The optical performance of the MDR is evaluated by using an optical vector analyzer (LUNA OVA CTe) to measure its transmission spectrum at the through port and drop port. Figure 4(a) shows the normalized transmission spectral response at the through (red) port and drop (blue) port of the fabricated MDR. The optical insertion loss at the through port is estimated to be 15.6 dB, most of which comes from the low coupling efficiency of the grating coupler. As can be seen, the transmission spectrum is clear and simple, only the first-order WGM is supported, which has an FSR of 30.26 nm. The measured transmission spectral response at the drop port has a larger optical insertion loss of 4.8 dB than that at the through port. The transmission peak of $WGM_{1,38}$ at the drop port has a 3 dB bandwidth of 0.87 nm, corresponding to a Q-factor of around 1.79×10^3, with an extinction ratio of 22.8 dB. When a DC voltage is applied and increased, due to the thermal-optic effect, the resonance wavelength of the MDR is redshifted. Figure 4(b) shows the $WGM_{1,38}$ resonance tuning of the MDR by increasing the DC voltage applied to the microheater. With the microheater power increasing from 0 to 19.35 mW, the resonance wavelength of the MDR is redshifted by 13.82 nm. During the redshift, the extinction ratio of the notch maintains almost unchanged. From the voltage–current measurement, the microheater resistance is estimated to be 629.4 Ω. Figure 4(c) shows the resonance wavelength shift of $WGM_{1,38}$ with the increase in the applied DC voltage. The wavelength shift rate is calculated to be 714.2 pm/mW. The key advantages of using the MDR in the implementation of the Fano device include an ultracompact size and a strong thermal tunability with ultralow power consumption.

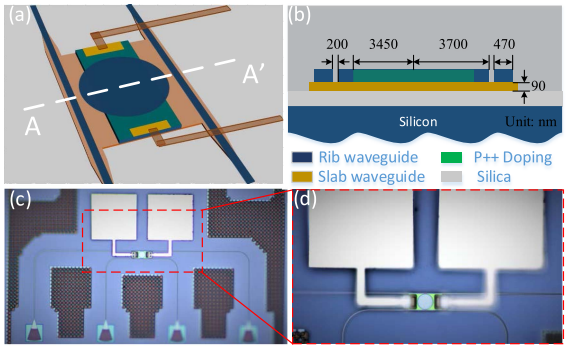

Fig. 3. (a) Perspective view of the add–drop MDR with a doped microheater. (b) Cross-sectional view of the MDR along the white dashed line AA′ shown in (a). (c) Image of the fabricated stand-alone MDR. (d) Zoom-in view of the add–drop MDR.

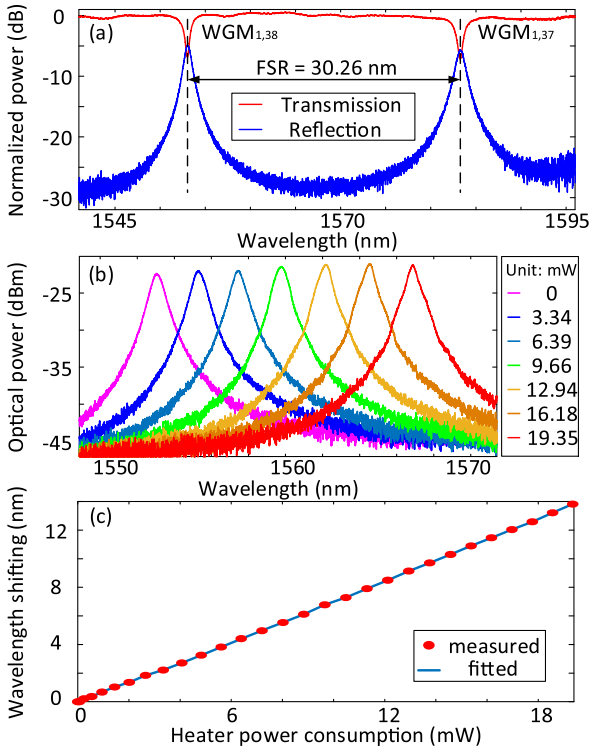

Fig. 4. (a) Normalized transmission spectral responses at the through (red) and drop (blue) port of the fabricated MDR. (b) Resonance tuning of $WGM_{1,38}$ with different powers. (c) Resonance wavelength shift of $WGM_{1,38}$ with a tuning power from 0 to 19.35 mW.

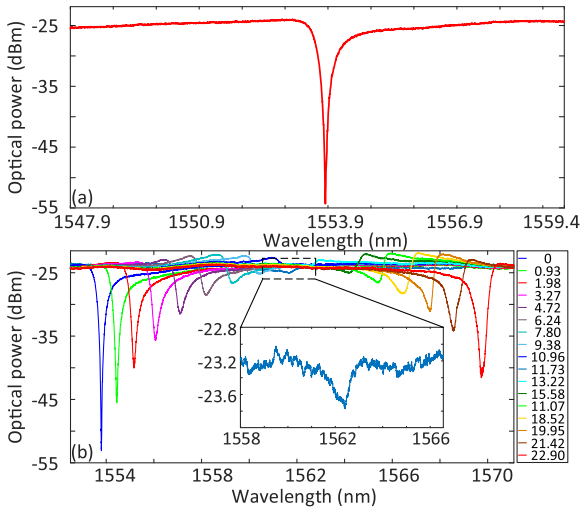

Fig. 5. (a) Measured Fano resonance when the fabricated device is in the static state. (b) Fano resonance tuning with the applied DC voltage increasing. Inset shows the measured transmission spectral response when the Fano parameter q is zero.

Then, the optical performance of the fabricated Fano device is evaluated. Since the optical vector analyzer is used to measure its transmission spectrum, the photodetector is not used in the measurement. Figure 5(a) shows the measured transmission spectrum when the device is in the static state. As can be seen, a Fano resonance with an asymmetric line shape is resulted, and its Fano parameter q is negative. The Fano resonance has an extinction ratio of 30.2 dB and a slope rate of 41 dB/nm. When a DC voltage is applied and increased, the Fano resonance is tuned and shifted to a longer wavelength. Figure 5(b) shows the tuning of the measured Fano resonance of the fabricated device. With the DC power increased from 0 to 22.9 mW, a maximum wavelength shift of the Fano resonance is measured to be 15.97 nm. As the resonance wavelength of the MDR is redshifted, the optical interference between the modes of the MDR and MZI is tuned, which leads to the tuning of the Fano resonance. It is clear to see in Fig. 5(b) when the Fano parameter q is tuned from negative to zero, its extinction ratio and slope rate becomes smaller, and when the Fano parameter q is tuned from 0 to positive, the extinction ratio and slope rate becomes larger, which matches well with the simulation results in Fig. 2(b) except the resonance wavelength is slightly drifted, which is caused by the fabrication imperfections. In addition, when the Fano parameter q is equal to zero, there is no optical interference between the modes of the MDR and the MZI, and only the resonance notch of the MDR is presented, as shown in the inset of Fig. 2(b). This experimental result confirms that by changing the optical interference between the resonant modes of the MDR and the MZI, the Fano resonance could be tuned.

In summary, a thermally tunable ultracompact Fano resonance device on a silicon photonic chip was proposed and demonstrated. In the device, an add–drop MDR was employed in which the through and drop ports were connected by two wire waveguides and combined by an adiabatic 2 × 2, 3 dB coupler to produce an MZI. Due to the resonant mode coupling between the MDR and the MZI, a Fano resonance with an asymmetric line shape was resulted. For thermal tuning, a *p*-type-doped microheater was incorporated in the MDR. With a DC voltage applied and increased, the Fano resonance was tuned. The device was designed, fabricated, and characterized. Measurement results showed a Fano resonance with an extinction ratio of 30.2 dB and a slope rate of 41 dB/nm were achieved. When the DC voltage applied to the microheater power was tuned with a tunable power from 0 to 22.9 mW, the Fano line shape was largely tuned with the Fano parameter q tuned from negative (−0.98) to positive (0.95) and a maximum wavelength shift of 15.97 nm. The key advantage of the proposed device is its ultracompact configuration and strong and fast tunability with low power consumption, which holds a high potential for applications in on-chip optical switching and sensing.

Funding. Natural Sciences and Engineering Research Council of Canada (NSERC).

Acknowledgment. This work is supported by the Natural Sciences and Engineering Research Council of Canada (NSERC) under the Silicon Electronic-Photonic Integrated Circuits (Si-EPIC) CREATE program. We acknowledge CMC Microsystems for providing the design tools and enabling the fabrication.

REFERENCES

1. U. Fano, Phys. Rev. **124**, 1866 (1961).
2. M. F. Limonov, M. V. Rybin, A. N. Poddubny, and Y. S. Kivshar, Nat. Photonics **11**, 543 (2017).
3. B. Luk'yanchuk, N. I. Zheludev, S. A. Maier, N. J. Halas, P. Nordlander, H. Giessen, and C. T. Chong, Nat. Mater. **9**, 707 (2010).
4. L. Stern, M. Grajower, and U. Levy, Nat. Commun. **5**, 4865 (2014).
5. F. Cheng, H. F. Liu, B. H. Li, J. Han, H. Xiao, X. F. Han, C. Z. Gu, and X. G. Qiu, Appl. Phys. Lett. **100**, 131110 (2012).
6. W. Zhou, D. Zhao, Y.-C. Shuai, H. Yang, S. Chuwongin, A. Chadha, J.-H. Seo, K. X. Wang, V. Liu, Z. Ma, and S. Fan, Prog. Quantum Electron. **38**, 1 (2014).
7. M. Rahmani, B. Luk'yanchuk, and M. Hong, Laser Photon. Rev. **7**, 329 (2013).
8. M. Hochberg and T. Baehr-Jones, Nat. Photonics **4**, 492 (2010).
9. A. Bera, M. Kuittinen, S. Honkanen, and M. Roussey, Opt. Lett. **43**, 3489 (2018).
10. C. M. Chang and O. Solgaard, Opt. Express **21**, 27209 (2013).
11. Z. Zhang, G. Nga, T. Hu, H. Qiu, X. Guo, W. Wang, M. Rouifed, C. Liu, and H. Wang, Appl. Phys. Lett. **111**, 081105 (2017).
12. A. C. Ruege and R. M. Reano, J. Lightwave Technol. **28**, 2964 (2010).
13. Y. Yu, M. Heuck, H. Hu, W. Xue, C. Peucheret, Y. Chen, L. K. Oxenlowe, K. Yuvind, and J. Mork, Appl. Phys. Lett. **105**, 061117 (2014).
14. W. Zhang and J. P. Yao, Opt. Lett. **41**, 2474 (2016).
15. T. Lin, X. Zhang, Y. Zou, F. Chau, J. Deng, and G. Zhou, Appl. Phys. Lett. **107**, 153107 (2015).
16. T. Lin, F. Chau, J. Deng, and G. Zhou, Appl. Phys. Lett. **107**, 223105 (2015).
17. T. Hu, P. Yu, C. Qiu, H. Qiu, F. Wang, M. Yang, X. Jiang, H. Yu, and J. Yang, Appl. Phys. Lett. **102**, 011112 (2013).
18. A. Li and W. Bogaerts, APL Photon. **2**, 096101 (2017).
19. Z. Zhang, G. Ng, T. Hu, H. Qiu, X. Guo, W. Wang, M. Rouifed, C. Liu, J. Sia, J. Zhou, C. Littlejohns, M. Nedeljkovic, G. T. Reed, and H. Wang, IEEE Photon. J. **10**, 6601108 (2018).
20. W. Zhang and J. P. Yao, J. Lightwave Technol. **35**, 4418 (2017).